

Ca2-VDM: Efficient Autoregressive Video Diffusion Model with Causal Generation and Cache Sharing

Kaifeng Gao^{1*}, Jiaxin Shi^{2*}, Hanwang Zhang³, Chunping Wang⁴, Jun Xiao¹, Long Chen⁵
¹Zhejiang University, ²Xmax.AI, ³Nanyang Technological University, ⁴Finvolution Group,
⁵The Hong Kong University of Science and Technology
¹ kite_phone@zju.edu.cn ² shijx12@gmail.com ⁵ longchen@ust.hk

Abstract

With the advance of diffusion models, today’s video generation has achieved impressive quality. To extend the generation length and facilitate real-world applications, a majority of video diffusion models (VDMs) generate videos in an autoregressive manner, i.e., generating subsequent clips conditioned on the last frame(s) of the previous clip. However, existing autoregressive VDMs are highly inefficient and redundant: The model must re-compute all the conditional frames that are overlapped between adjacent clips. This issue is exacerbated when the conditional frames are extended autoregressively to provide the model with long-term context. In such cases, the computational demands increase significantly (i.e., with a quadratic complexity w.r.t. the autoregression step). In this paper, we propose **Ca2-VDM**, an efficient autoregressive VDM with **Causal generation** and **Cache sharing**. For **causal generation**, it introduces unidirectional feature computation, which ensures that the cache of conditional frames can be precomputed in previous autoregression steps and reused in every subsequent step, eliminating redundant computations. For **cache sharing**, it shares the cache across all denoising steps to avoid the huge cache storage cost. Extensive experiments demonstrated that our Ca2-VDM achieves state-of-the-art quantitative and qualitative video generation results and significantly improves the generation speed. Code is available at <https://github.com/Dawn-LX/CausalCache-VDM/>

1. Introduction

Video diffusion models (VDMs) [12, 21, 24, 32] have made significant advancements by benefiting from the powerful diffusion techniques [16, 37, 38] and prior studies on image

*Kaifeng Gao and Jiaxin Shi have equal contributions. Part of the work was done when Kaifeng Gao served as a visiting Ph.D. student at The Hong Kong University of Science and Technology.

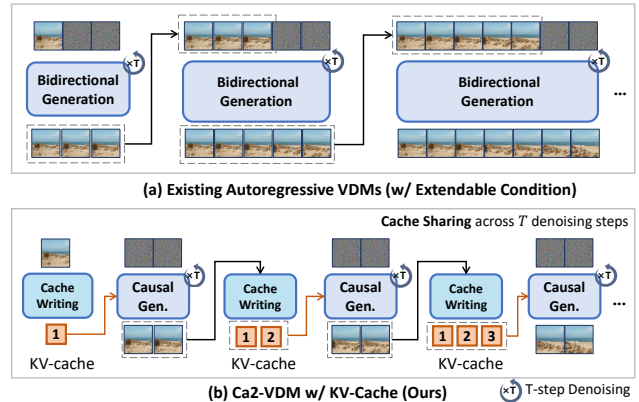


Figure 1. (a): Existing autoregressive VDMs with **bidirectional generation**. The conditional frames can be fixed-length [15, 55] or extendable. (b): Our Ca2-VDM, which uses **causal generation** to enable KV-cache and introduce **cache sharing** across all denoising timesteps. **Cache writing** stands for a partial model forward on the denoised frames (i.e., at timestep $t = 0$) until the KV-caches of every layer are computed.

generation [4, 29, 33]. In contrast to images, VDMs need to capture interactions across multiple frames and generate all frames simultaneously (e.g., a 16-frame clip). This is usually facilitated by the temporal attention in prevailing UNet- or Transformer-based VDMs [24, 43]. They introduce interdependencies during the bidirectional attention computation. Consequently, the training and inference lengths must be aligned, extremely restricting the flexibility of VDMs in real-world applications such as long-term [15] or live-stream [1] video generation. Meanwhile, simply scaling the clip length at inference time breaks the alignment and leads to poor generation quality (e.g., Figure 1(b) in [30]), unless one undertakes time-consuming retraining or fine-tuning.

To address this issue, an effective and prevalent solution is **autoregressive VDMs** [2, 15, 21]: They are capable of autoregressively generating subsequent clips conditioned

on last frame(s)¹ of previous clip, as shown in Figure 1(a). However, the autoregression process of existing VDMs is highly *inefficient and redundant*: The conditional frames constitute the overlapping frames between adjacent autoregression chunks and they are re-computed at each step. This issue is exacerbated when the conditional frames are extended autoregressively to provide the model with long-term context. In such cases, the model must re-compute all the conditional frames concatenated by the previously generated chunks, with a quadratic computational demand w.r.t. the autoregressive step (*cf.* Figure 8 in Sec. 4.3).

To overcome the above limitations, we propose to cache the intermediate features (specifically, the keys and values of every attention layer) at each autoregression (AR) step, and reuse them in subsequent AR steps, as shown in Figure 1(b). In this way, the model 1) eliminates the redundant computations in temporal attention blocks, and 2) reduces the processing length to a constant for other temporal-parallel blocks (*e.g.*, spatial attention and visual-text cross attention) while maintaining the extendable long-term context. To successfully implement the KV-cache in VDMs, two key factors must be carefully considered:

- **Cache Computation.** In existing VDMs, the temporal attention is bidirectional, as shown in Figure 2(a). The frames $z_t^{3,4}$ are denoised conditioned on $z_0^{0,1,2}$, and key/value features of $z_0^{0,1,2}$ are also computed conditioned on $z_t^{3,4}$ at every diffusion timestep t (highlighted by the red box and arrows). It’s impossible to precompute and cache the keys and values of $z_0^{0,1,2}$ at previous AR steps, since $z_t^{3,4}$ are not yet available.
- **Cache Storage.** During inference, the VDM is repeatedly called in the denoising process at each AR step, where each call is taken with a different timestep t . All most all Existing VDMs [21, 32] use the same timestep embedding (indexed by t) for both conditional and noisy frames. This requires each denoising step to have its own cache, *i.e.*, caching the key/value features for all denoising steps will consume huge GPU memory.

In this paper, we propose an efficient autoregressive VDM boosted by causal generation and cache sharing, termed Ca2-VDM, to handle both challenges. For cache computation, we propose **causal generation**: We replace the full temporal attention in each block of the VDM with *causal* temporal attention, and propose *prefix-enhanced* spatial attention. The former ensures each generated frame only depends on its prefix frames, and the latter enhances the guidance from the prefix frames. As a result, the cache to be used in subsequent autoregression steps can be precomputed at early steps. For cache storage, we propose **cache sharing**. It leverages the advantages of causal generation: The cache is determined only by the non-noisy preceding (conditional) frames and unaffected by the subsequent noisy

¹Image-to-video models can be considered as a special case.

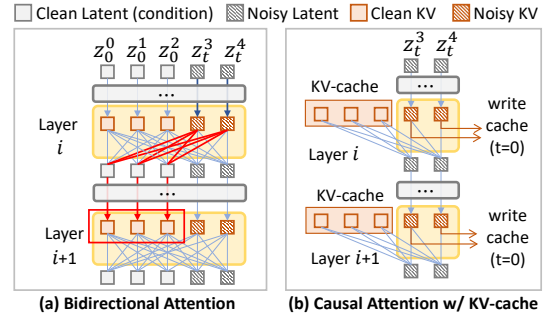


Figure 2. Comparison of bidirectional attention (a) and causal attention (ours) (b). Our design addresses the **cache computation** and **cache storage** issues.

frames (*i.e.*, independent of the timestep t). Thus, by using a distinct timestep embedding indexed by $t = 0$ for the conditional frames in both training and inference, we enable the cache to be shared across all the denoising steps.

Equipped with causal generation and cache sharing, we propose to store the KV-cache in a queue so that the model can exploit the long-term context while maintaining an affordable computation and storage cost. To support this queue design, the training samples are partially noised to keep clean prefix frames (with random length) as the condition, and the maximum condition length covers the length of KV-cache queue at inference time. Meanwhile, sinusoidal spatial and temporal positional embeddings (*i.e.*, SPEs and TPEs) are added to the frame sequence following Vision Transformer (ViT) [7]. During inference, the TPEs are assigned chunk-by-chunk as the autoregression progresses. To ensure TPEs are correctly assigned when the cumulatively generated video exceeds the training length, we carefully design a cyclic shift mechanism: *Cyclic-TPEs*².

We evaluated our Ca2-VDM on multiple public datasets including MSR-VTT [47], UCF-101 [39], and Sky Time-lapse [51] for both text-to-video and video prediction tasks. The results show that our model achieves significant inference speed improvement while maintaining comparable quantitative and qualitative performance as state-of-the-art VDMs. In summary, we make three contributions in this paper: 1) A causal generation structure that allows the intermediate features of conditional frames can be cached and reused in every autoregression step, eliminating the redundant computation. 2) A cache sharing strategy implemented on the KV-cache queue and facilitated by *Cyclic-TPEs*. It allows the model to acquire extendable context while significantly reducing the storage cost. 3) Our Ca2-VDM achieves comparable performance with SOTA VDMs at a much less computation demand and a high inference speed.

²Originally, TPEs are re-assigned from scratch at each AR step. However, when KV-cache is enabled, early TPEs have been **bound** to previous KV-caches. They can not be re-assigned (*cf.* Figure 4(c) for more details).

2. Related Work

Video Diffusion Models (VDMs) have shown impressive generation capabilities, building on the success of latent diffusion models in image generation applications [4, 29, 33]. Some works [17, 19, 22, 54] develop training-free methods for zero-shot video generation based on pretrained image diffusion models (e.g., Stable Diffusion [33]). To leverage video training data and improve the generation quality, many works [6, 9, 12, 32, 43] extend the 2D Unet in text-to-image diffusion models with temporal attention layers or temporal convolution layers. Recent studies [21, 24] also build VDMs based on spatial-temporal Transformers due to their inherent capability of capturing long-term temporal dependencies. We build our Ca2-VDM based on spatial-temporal Transformers following prior structures.

Tuning-free Video Extrapolation. Prior studies have explored autoregressively extrapolating videos using pretrained short video diffusion models without additional finetuning. These methods usually consist of initializing noise sequence based on the DDIM inversion [25, 37] of previously generated frames [28], co-denoising overlapped short clips [42], or iteratively denoising short clips with noise-rescheduling [30]. However, their generation quality is upper-bounded by the pretrained VDMs. Meanwhile, the lack of finetuning also leads to temporal inconsistencies between short clip transitions.

Past-frame Conditioned Video Prediction. To enhance generation quality and temporal consistency, a popular paradigm is training VDMs conditioned on past frames to predict future frames, enabling video extrapolation through autoregressive model calls. Recent works of autoregressive VDMs have studied a variety of design choices for injecting conditional frames, such as adaptive layer normalization [21, 41], cross-attention [15, 21, 53], and explicitly concatenating to the noisy latent along the temporal-axis [13, 21] or channel-axis [5, 10, 50]. Some works [11, 46] also inject conditional frames by adapter-like subnets (e.g., T2I-adapter [26] or ControlNet [52]). In contrast to existing works, our Ca2-VDM avoids the redundant computation of conditional frames by causal generation and cache sharing, and significantly improves the generation speed.

3. Method

3.1. Preliminaries and Problem Formulation

Preliminaries. Diffusion Models [16, 36] are generative models that model a target distribution $\mathbf{x}_0 \sim q(\mathbf{x}_0)$ by learning a denoising process with arbitrary noise levels. To do this, a diffusion process is defined to gradually corrupt \mathbf{x}_0 with Gaussian noise. Each diffusion step is $q(\mathbf{x}_t|\mathbf{x}_{t-1}) = \mathcal{N}(\mathbf{x}_t; \sqrt{1 - \beta_t}\mathbf{x}_{t-1}, \beta_t\mathbf{I})$, where $t = 1, \dots, T$ and $\beta_t \in (0, 1)$ is the variance schedule. By applying the reparameterization trick [16], each \mathbf{x}_t can be sam-

pled as $\mathbf{x}_t = \sqrt{\bar{\alpha}_t}\mathbf{x}_0 + \sqrt{1 - \bar{\alpha}_t}\epsilon_t$, where $\epsilon_t \sim \mathcal{N}(\mathbf{0}, \mathbf{I})$ and $\bar{\alpha}_t = \prod_{i=1}^t(1 - \beta_i)$. Given the diffusion process, a diffusion model is then trained to approximate the reverse process (denoising process). Each denoising step is parameterized as $p_\theta(\mathbf{x}_{t-1}|\mathbf{x}_t) = \mathcal{N}(\mathbf{x}_{t-1}; \boldsymbol{\mu}_\theta(\mathbf{x}_t, t), \boldsymbol{\Sigma}_\theta(\mathbf{x}_t, t))$, where θ contains learnable parameters.

Problem Formulation. Following existing mainstream VDMs [12, 21, 24], we develop Ca2-VDM based on latent diffusion models [33] to reduce the modeling complexity of high dimensional visual data. This is achieved by using a pretrained variational autoencoder (VAE) encoder \mathcal{E} to compress \mathbf{x}_0 into a lower-dimensional latent representation, i.e., $\mathbf{z}_0 = \mathcal{E}(\mathbf{x}_0)$. Consequently, the diffusion and denoising processes are implemented in the latent space, formulated as $q(\mathbf{z}_t|\mathbf{z}_{t-1})$ and $p_\theta(\mathbf{z}_{t-1}|\mathbf{z}_t)$, respectively. The denoised latent $\hat{\mathbf{z}}_0$ is decoded back to the pixel space by the pretrained VAE decoder \mathcal{D} , i.e., $\hat{\mathbf{x}}_0 = \mathcal{D}(\hat{\mathbf{z}}_0)$.

In our setting, the model takes as input a VAE encoded latent sequence³ $\mathbf{z}_0^{0:L} = [\mathbf{z}_0^0, \dots, \mathbf{z}_0^{L-1}] \in \mathbb{R}^{L \times H \times W \times C}$, where L is the number of frames, $H \times W$ is the downsampled resolution, and C is the number of channels. Then, it aims to generate future frames conditioned on past frames, by learning a distribution $p_\theta(\mathbf{z}_0^{P:L}|\mathbf{z}_0^{0:P})$. Here the first P prefix frames serve as condition (referred to as **clean prefix**), and the remaining $L - P$ frames are those to be denoised (referred to as **denoising target**). The model parameterized by θ is denoted as $\epsilon_\theta(\mathbf{z}_0^{0:L}, t)$.

The overall pipeline of Ca2-VDM is shown in Figure 3. We first illustrate the **causal generation** in the training stage (Sec. 3.2), as well as the training objectives. Then, we introduce the KV-cache realization combined with the **cache sharing** mechanism in the autoregressive inference stage (Sec. 3.3), and the queue structure for temporal KV-cache supported by Cyclic-TPEs (cf. Figure 4).

3.2. Causal Generation and Training Objectives

We first introduce the training objectives, followed by an elaboration of the causal generation block (cf. Figure 3(c)). Here we mainly illustrate the causal temporal attention and prefix-enhanced spatial attention layers. As for the visual-text cross attention, it is widely used in VDMs for text-to-video generation [4, 33]. And it is optional for pure video prediction [21]. Since it is not our primary focus, we refer readers to related works [4, 33] for more details.

Training Objectives. Existing diffusion models [16, 27, 29] are trained with the variational lower bound of \mathbf{z}_0 's log-likelihood, formulated as $\mathcal{L}_{\text{vib}}(\theta) = -\log p_\theta(\mathbf{z}_0|\mathbf{z}_1) + \sum_t D_{KL}(q(\mathbf{z}_{t-1}|\mathbf{z}_t, \mathbf{z}_0)||p_\theta(\mathbf{z}_{t-1}|\mathbf{z}_t))$, where D_{KL} is determined by the mean $\boldsymbol{\mu}_\theta$ and covariance $\boldsymbol{\Sigma}_\theta$. By reparameterizing $\boldsymbol{\mu}_\theta$ as a noise prediction network ϵ_θ and fixing $\boldsymbol{\Sigma}_\theta$ as a constant variance schedule [16], the model can

³Throughout this paper, we use " $a : b$ " to denote a half-open interval ranging from a (inclusive) to b (exclusive)

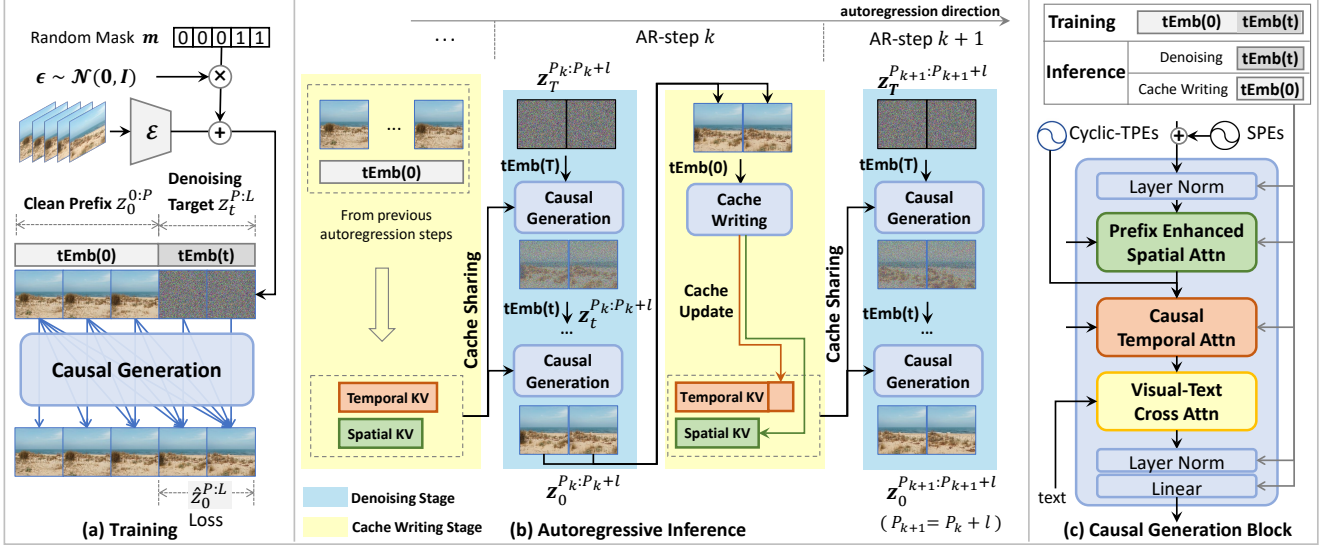


Figure 3. Overview of the Ca2-VDM pipeline. (a): During training, we randomly set P frames clean prefix, and set distinctive timestep embeddings, *i.e.*, $\mathbf{tEmb}(0)$ for the clean prefix and $\mathbf{tEmb}(t)$ for the denoising target. (b): During inference, in each autoregression (AR) step, the model denoises an l -frame chunk conditioned on the spatial/temporal KV-caches shared across all timesteps (denoising stage), and then computes the keys/values of denoised chunk to update the KV-caches (cache writing stage). (c): Causal generation block. We further illustrate the details of causal temporal attention with Cyclic-TPEs in Figure 4 and the prefix-enhanced spatial attention in Figure 5.

be trained using a simplified objective function:

$$\mathcal{L}_{\text{simple}}(\theta) = \mathbb{E}_{z, \epsilon, t} [\|\epsilon_{\theta}(z_t, t) - \epsilon\|_2^2], \quad \epsilon \sim \mathcal{N}(0, 1). \quad (1)$$

In our setting, each sample is partially noised. We randomly keep P consecutive frames uncorrupted as the clean prefix, and the remaining frames are treated as the denoising target, as shown in Figure 3(a). We use different timestep embeddings for the clean prefix (*i.e.*, $\mathbf{tEmb}(0)$) and the denoising target (*i.e.*, $\mathbf{tEmb}(t)$), rather than a unified timestep embedding for the whole video clip as in many existing VDMs [21, 24]. This ensures the cache from the clean prefix can be correctly shared across each denoising timestep t at inference time (since the clean prefix is always assigned with $\mathbf{tEmb}(0)$). Consequently, the simplified objective function for our model is

$$\tilde{\mathcal{L}}_{\text{simple}}(\theta) = \mathbb{E}_{z, \epsilon, t} [\|(\epsilon_{\theta}([z_0^{0:P}, z_t^{P:L}], t) - \epsilon) \odot \mathbf{m}\|_2^2], \quad (2)$$

where $[\cdot, \cdot]$ stands for concatenation along the temporal axis, and t is the timestep vector with $t_i = t$ if $i \geq P$ else 0. $\mathbf{m} \in \{0, 1\}^N$ is a loss mask to exclude the clean prefix part, *i.e.*, with $m_i = 1$ if $i \geq P$ else 0. In practice, we train the model with learnable covariance Σ_{θ} by optimizing a combination of $\tilde{\mathcal{L}}_{\text{simple}}$ and \mathcal{L}_{vib} (with the same loss mask) following [27, 29]. More details are left in the Appendix.

Causal Temporal Attention. To introduce the causality, we mask the attention map to force each frame to only attend to its preceding frames, as shown in Figure 4(a). Specifically, the input to each layer is first permuted by

treating the spatial resolution $H \times W$ as the batch dimension, and then linearly projected to query, key, and value features as $\mathbf{Q}, \mathbf{K}, \mathbf{V} \in \mathbb{R}^{L \times C'}$ (for every spatial grid). The causal attention is computed as (we only describe one attention head and omit the diffusion step t for brevity):

$$\text{CausalAttn}(\mathbf{Q}, \mathbf{K}, \mathbf{V}) = \text{Softmax}\left(\frac{\mathbf{Q}\mathbf{K}^T}{\sqrt{C'}} + \mathbf{M}\right) \mathbf{V}, \quad (3)$$

where $\mathbf{M} \in \mathbb{R}^{L \times L}$ is a lower triangular attention mask with $M_{i,j} = -\infty$ if $i < j$ else 0.

Prefix-Enhanced Spatial Attention. In analogy to causal temporal attention, integrating the clean prefix and denoising target into one attention sequence helps enhance the guidance of conditional information. Inspired by prior works [18, 32], we do this via spatial-wise concatenation, as shown in Figure 5. Let $\mathbf{h}_t^{0:L} \in \mathbb{R}^{L \times H \times W \times C'}$ be the hidden input to each layer, where the number of frames L is treated as batch dimension and $H \times W$ is flattened for attention calculation. We take a sub-prefix of length P' and concatenate it to the denoising target. Specifically, for \mathbf{h}_t^i from the i -th frame, the query is calculated as $\bar{\mathbf{Q}}(i) = \mathbf{W}^Q \mathbf{h}_t^i$. The prefix-enhanced key is calculated as

$$\bar{\mathbf{K}}(i) = \begin{cases} \mathbf{W}^K [\mathbf{h}_0^{P-P'}, \dots, \mathbf{h}_0^{P-1}, \mathbf{h}_t^i] & \text{if } i \geq P \\ \mathbf{W}^K [\mathbf{h}_0^i, \dots, \mathbf{h}_0^i] & \text{if } i < P \end{cases}, \quad (4)$$

where $[\cdot; \cdot]$ stands for concatenation along the spatial dimension, and \mathbf{h}_0^i is broadcasted by self-repeat P' times for every $i < P$ (*i.e.*, the clean prefix part). We do the same

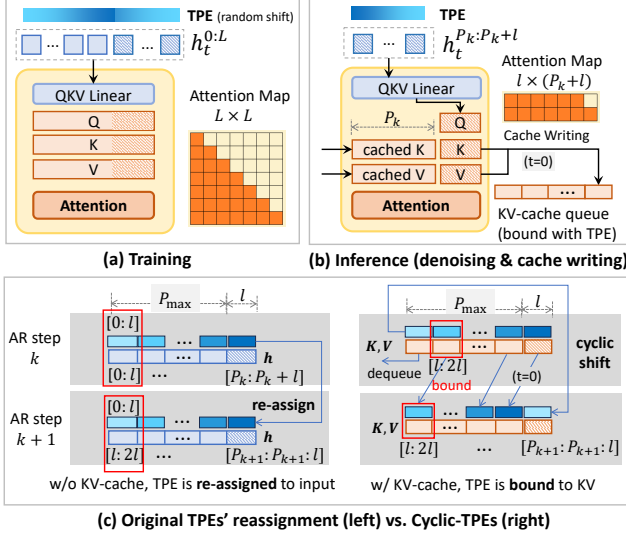


Figure 4. Illustration of causal temporal attention (a) & (b) and the temporal KV-cache queue with Cyclic-TPEs (c). In (c), assume that $L_{\text{train}} = P_{\text{max}} + l$ and $P_{k+l} = P_k + l$. We show the state that autoregressive inference reaches $P_k = P_{\text{max}}$.

operation to obtain the prefix-enhanced value \tilde{V} . Consequently, for every frame, the prefix-enhanced spatial attention is computed as $\text{Attention}(\tilde{Q}, \tilde{K}, \tilde{V})$ with an attention map of shape $(HW) \times ((P' + 1)HW)$. In practice, we set P' relatively small (e.g., $P' = 3$), as the computational cost scales proportionally with P' , while adjacent prefix frames tend to exhibit similar appearances. We empirically show that prefix enhancement improves the quality of autoregressive generation (cf. Table 3 in Sec. 4.2).

3.3. Autoregressive Inference with Cache Sharing

We first introduce an overview of the autoregressive inference equipped with cache sharing, as shown in Figure 3(b). Then for each autoregression step, we illustrate the temporal KV-cache queue and cyclic temporal positional embeddings (Cyclic-TPEs). Finally, we introduce the spatial KV-cache for prefix-enhanced spatial attention.

Autoregressive Inference. The model starts from a given first frame and generates an l -frame chunk per AR step. Each AR step consists of a denoising stage and a cache writing stage. The spatial and temporal KV-caches are shared across every denoising timestep t (i.e., cache sharing). In the denoising stage, given P_k generated frames at AR step k , each denoising step samples $z_t^{P_k:P_k+l} \sim p_\theta(z_t^{P_k:P_k+l} | z_t^{P_k:P_k+l}, z_0^{0:P_k})$. Here $z_0^{0:P_k}$ serves as the clean prefix and $z_t^{P_k:P_k+l}$ is the denoising target. Benefiting from the causal generation, the feature computation is unidirectional. This means $z_t^{P_k:P_k+l}$ is denoised conditioned on $z_0^{0:P_k}$ while the cache of $z_0^{0:P_k}$ could be precomputed in previous autoregression steps without referring to $z_t^{P_k:P_k+l}$.

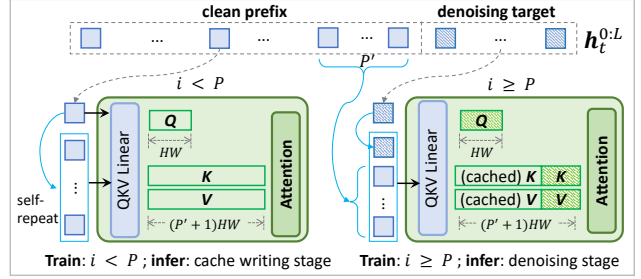


Figure 5. Illustration of prefix-enhanced spatial attention. For $i \geq P$, the left part of K, V is from clean prefix (in training) or cached K, V (in the denoising stage of inference).

In the cache writing stage, the denoised $z_0^{P_k:P_k+l}$ is input to the model again to compute its *clean* spatial and temporal KV-caches, which will be used in the next AR step.

Temporal KV-Cache. Suppose that there are P_k generated frames (i.e., the clean prefix) at AR step k . In the denoising stage, the query, key, and value features at timestep t are $Q_t^{P_k:P_k+l}, K_t^{P_k:P_k+l}, V_t^{P_k:P_k+l} \in \mathbb{R}^{l \times C'}$ (considering only one spatial grid). The model reads the *clean* key and value caches as $K_0^{0:P_k}, V_0^{0:P_k} \in \mathbb{R}^{P_k \times C'}$. Then, they are concatenated to the noisy ones as $\tilde{K}(k, t) = [K_0^{0:P_k}, K_t^{P_k:P_k+l}]$ and $\tilde{V}(k, t) = [V_0^{0:P_k}, V_t^{P_k:P_k+l}]$. Finally, the causal temporal attention is computed as:

$$\text{CausalAttn}(Q_t^{P_k:P_k+l}, \tilde{K}(k, t), \tilde{V}(k, t)), \quad (5)$$

where the attention map has a shape of $l \times (P_k + l)$, as shown in Figure 4(b). During denoising, the clean KV-cache $K_0^{0:P_k}$ and $V_0^{0:P_k}$ are shared for every timestep t . In the cache writing stage, the clean temporal keys and values are computed as $K_0^{P_k:P_k+l}$ and $V_0^{P_k:P_k+l}$. They are then updated into the KV-cache queue, resulting in $K_0^{0:P_{k+1}}$ and $V_0^{0:P_{k+1}}$, which will be used in AR step $k + 1$ (i.e., $P_{k+1} = P_k + l$). As the autoregression progresses, the earliest KV-cache will be dequeued when the length of the clean prefix P_k reaches a predefined P_{max} (i.e., a maximum number of conditional frames), as shown in Figure 4(c).

Cyclic-TPEs. Assume that the model was trained on video clips with a maximum length of $L_{\text{train}} = P_{\text{max}} + l$ (i.e., with P_{max} frames clean prefix and l frames denoising target). L_{train} is also the maximum length of TPE sequence during training. As the autoregressive inference progresses till $P_k = P_{\text{max}}$, the TPEs are used up. When KV-cache is disabled (cf. Figure 4(c)-left), to align the training pattern, we can re-assign the TPEs from scratch after the earliest clean frames are dequeued. However, when KV-cache is enabled (cf. Figure 4(c)-right), the TPEs were *bound* to keys and values at previous AR steps and had been stored in preceding KV-cache chunks. As a result, we cannot do reassignment to match the training pattern of TPEs. Here we introduce a cyclic shift mechanism, where the denoising



Figure 6. Qualitative examples generated by GenLV [42], StreamT2V [15], OS-Fix, and our Ca2-VDM. We sampled 32 frames with an interval of 8 frames for display. Note that GenLV does not strictly follow the given first frame, since it was not finetuned on explicitly injected conditional frames. In the implementation of GenLV, we used DDIM inversion to build the initial noise based on the first frame.

target will be assigned those TPEs indexed from the beginning. To support the training/inference alignment of Cyclic-TPEs, in the training stage, each sample is assigned a TPE sequence that is cyclically shifted with a random offset.

Spatial KV-Cache. Let $h_t^{P_k:P_k+l}$ be the input to the prefix-enhanced spatial attention at AR step k . In the denoising stage, the keys and values from the denoising target are enhanced by the spatial KV-cache (a sub-prefix of P' frames) via spatial-wise concatenation. In the cache writing stage, the denoised latent frames are first enhanced via self-repeat and then computed to obtain the clean spatial keys and values. These operations are aligned with the prefix-enhancement in Eq. (4) of the training stage. Since P' is relatively small ($P' < l$), the prefix enhancement for the current denoising target $h_t^{P_k:P_k+l}$ only depends on spatial KV-cache from the most recent generated chunk (*i.e.*, $h_0^{P_k-l:P_k}$). Thus, in contrast to the queue structure for temporal KV-cache, we only store the spatial KV-cache for one chunk and overwrite it at every AR step.

Discussion. It's worth noting that our KV-cache queue for autoregressive VDMs is not a trivial extension of the KV-cache techniques from large language models (LLMs): 1) LLMs predict the next token at each AR step, and the KVs are computed and cached *simultaneously* in each forward call. For VDMs, however, the model is repeatedly called during denoising (with different t). This brings the cache computation and storage issues as introduced in Sec. 1. Our implementation solves these two issues, sharing the cache across every denoising step. 2) Caching visual KVs costs much more storage than KVs for text since each token in our setting corresponds to HW visual grids. The queue structure for KV-cache is essential for VDMs considering this heavy storage cost. Early KVs can be safely dequeued as the appearance and motion of new frames are

primarily influenced by the most recent KVs. Meanwhile, we propose Cyclic-TPEs to facilitate this mechanism.

4. Experiments

4.1. Experimental Setup

Model Details and Baselines. We built Ca2-VDM based on spatial-temporal Transformer following [4, 24] and initialized it with Open-Sora v1.0 [55]. Following PixArt- α [4], we used T5 [31] as the text encoder and used the VAE from StableDiffusion [33]. The length of the clean prefix was randomly sampled according to the multiples of chunk length l , *i.e.*, $P \in \{1, 1+l, \dots, 1+nl\}$ and $P_{\max} = 1+nl$. We used training videos of various lengths with $L_{\text{train}} = P+l$. As comparisons, we built two bidirectional baselines (*cf.* Figure 1(a)) based on the same Open-Sora v1.0: One was trained with fixed-length conditional frames (denoted as OS-Fix), where P is fixed as $P = L_{\text{train}}/2$ in training and inference. The other was trained with autoregressively extendable conditional frames using the same training configs as Ca2-VDM (denoted as OS-Ext).

Training Details We conducted training on the text-to-video (T2V) generation and video prediction (*i.e.*, without text prompt) tasks. For T2V generation, we trained OS-Fix and Ca2-VDM on a large-scale video-text dataset InternVid [45], by filtering it to a sub-set of 4.9M high-quality video-text pairs. The models were trained video clips at resolution 256×256 with $l=16$ and $P_{\max} = 1 + 3l = 49$. For video prediction, we trained OS-Fix, OS-Ext, and Ca2-VDM on the SkyTimelapse [51] dataset at resolution 256×256 with $l=8$. OS-Ext and Ca2-VDM both used $P_{\max} = 1 + 3l = 25$. OS-Fix used a fixed $P = 8$. More details and hyperparameters are left in the Appendix.

Evaluation Datasets and Metrics. We used MSR-

Table 1. Zero-shot FVD scores on MSR-VTT [47] and UCF101 [39] test sets. All methods generate video at a resolution of $16 \times 256 \times 256$. C: condition. T and I are text and image conditions, respectively.

Method	C	MSR-VTT	UCF101
ModelScope [43]	T	550	410
VideoComposer [44]	T	580	-
Video-LDM [3]	T	-	550.6
PYoCo [9]	T	-	355.2
Make-A-Video [34]	T	-	367.2
AnimateAnything [6]	T+I	443	-
PixelDance [50]	T+I	381	242.8
SEINE [5]	T+I	181	-
Ca2-VDM	T+I	181	277.7

Table 2. Finetuned FVD scores on UCF-101 [39] test set. Methods with * were trained on both train and test sets.

Method	Res.	FVD
MCVD [41]	64^2	1143
VDT [21]	64^2	225.7
DIGAN* [48]	128^2	577
TATS [8]	128^2	420
VideoFusion [23]	128^2	220
LVDM* [14]	256^2	372
PVDM [49]	256^2	343.6
Latte [24]	256^2	333.6
Ca2-VDM	256^2	184.5

Table 3. Ablations of P_{\max} and prefix-enhancement (PE) on Sky-Timelapse [51]. Each variant of Ca2-VDM generated 48 frames with 6 AR steps. The results were divided into three 16-frame chunks for FVD evaluation.

P_{\max}	PE	Chunk Id		
		1	2	3
25	×	274.8	244.5	275.1
25	✓	257.4	216.5	238.5
41	×	187.3	209.3	263.2
41	✓	185.0	202.9	240.5

Table 4. FVD results on MSR-VTT [47] test set.

Method	FVD between AR step 1 and i				
	$i = 2$	$i = 3$	$i = 4$	$i = 5$	$i = 6$
GenLV [42]	282.8	291.4	299.0	318.2	310.3
StreamT2V [15]	317.5	434.7	478.2	462.0	512.4
OS-Fix	182.9	210.6	260.8	284.3	315.1
Ca2-VDM	160.6	206.5	262.8	281.3	304.7

VTT [47], UCF101 [39], and SkyTimelapse [51] datasets at resolution 256×256 , and reported Fréchet Video Distance (FVD) [40] following previous works [5, 9, 50]. More details about choosing text prompts and computing FVD scores on these datasets are left in the Appendix.

4.2. Evaluation for Generation Quality

We first compared the in-chunk generation quality of Ca2-VDM with SOTA VDMs. Then, we evaluated the temporal consistency of the autoregressive generation. Finally, we conducted ablation studies on Ca2-VDM’s design choices.

In-Chunk Generation Quality. We evaluated the zero-shot text-to-video (T2V) FVD scores on MSR-VTT [47] and UCF101 [39], as shown in Table 1. We compared Ca2-VDM to state-of-the-art T2V models including two groups: 1) Text conditioned: ModelScope [43], VideoComposer [44], Video-LDM [3], PYoCO [9], and Make-A-Video [34]. 2) Text with extra image conditioned, *e.g.*, for image-to-video: AnimateAnything [6], PixelDance [50] and video transition: SEINE [5]. We also finetuned Ca2-VDM on UCF101 at resolution $16 \times 256 \times 256$ and reported the FVD scores in Table 2. We compared it with SOTA video generation models: MCVD [41], VDT [21], DIGAN [48], TATS [8], LVDM [14], PVDM [49], and Latte [24]. The FVD results in both Table 1 and Table 2 show that our Ca2-VDM has a competitive T2V performance with SOTA models. We further show some qualitative examples in Figure 6. We can see that Ca2-VDM has comparable generation quality with existing SOTA models.

Temporal Consistency. We compared Ca2-VDM with

the two baselines (*i.e.*, OS-Fix and OS-Ext) and existing SOTA autoregressive VDMs. To the best of our knowledge, existing autoregressive VDMs all use fixed-length conditional frames (similar to OS-Fix). We used GenL-Video (GenLV) [42] and StreamT2V [15]. Specifically, GenLV utilizes a base model AnimateDiff [12] and conducts co-denosing for overlapped 16-frame clips. We implemented it with an overlapping length (*i.e.*, the condition length) of 8 frames. StreamT2V is based on Stable Video Diffusion (SVD) [2] and finetunes it conditioned on preceding frames to generate subsequent frames. It also generates 16 frames at each AR step, with 8 frames as the condition.

We evaluated the FVD scores of each autoregression (AR) chunk w.r.t. the first chunk, as shown in Table 4. We can observe that Ca2-VDM has relatively lower FVD scores than the others. This indicates that extendable (long-term) condition helps to improve the temporal consistency. We also show qualitative examples in Figures 7. It shows content mutations in consecutive frames from the results of fixed-length condition methods, *e.g.*, the 24th and 25th frames in GenLV, and the 65th and 66th frames in StreamT2V. We further compared Ca2-VDM with the condition extendable baseline, *i.e.*, OS-Ext (*cf.* Figure 9). We see that Ca2-VDM shows comparable results with OS-Ext (while being more computationally efficient as demonstrated in the following Sec. 4.3).

Ablation Studies. We studied the effectiveness of longer condition length and the prefix-enhancement (PE) in spatial attention (*cf.* Eq. (4)). We trained variants of Ca2-VDM with different P_{\max} or without PE. The results are reported in Table 3. Each model was called with 6 AR steps to generate a 49-frame video (with the given first frame) and evaluated by the FVD scores of three 16-frame chunks (exclude the first frame) w.r.t. the 16-frame ground-truth videos. We can see that both increasing P_{\max} and using PE are beneficial in improving the generation quality.



Figure 7. Qualitative examples from GenLV [42], StreamT2V [15], OS-Fix, and our Ca2-VDM. Yellow arrows highlight the consecutive frames having mutations.

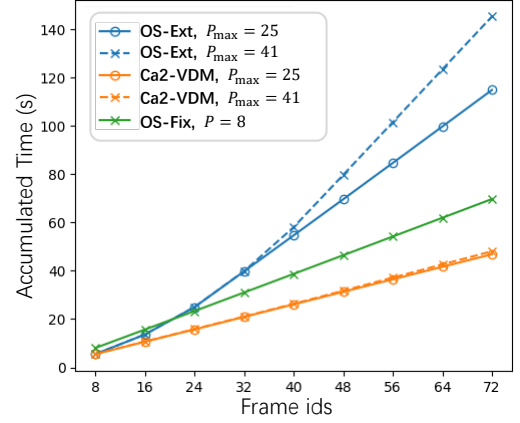


Figure 8. Accumulated time cost *w.r.t.* frame ids. We show OS-Ext and Ca2-VDM with $P_{\max} = 25$ and 41, and OS-Fix with a fixed $P = 8$.

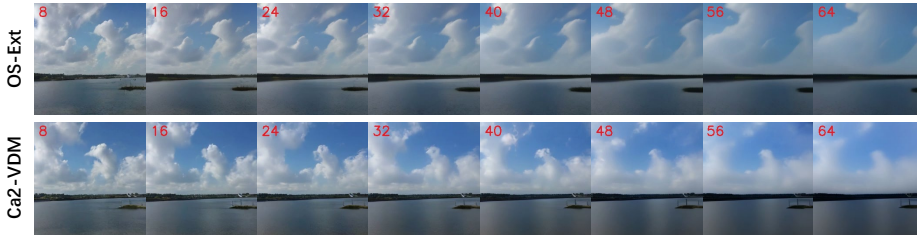


Figure 9. Results from OS-Ext and Ca2-VDM. They have comparable quality, while Ca2-VDM is more efficient in autoregressive generation, as evidenced in Table 5, Figure 8 and 10.

Table 5. Cumulative time cost for autoregressively generating 80 frames at resolution 256×256 . Ext.C. means extendable condition. OS-Fix used $P=8$. OS-Ext and Ca2-VDM used $P_{\max}=25$.

Method	Ext.C.	Time (s)
StreamT2V [15]		150
OS-Ext	✓	130.1
OS-Fix		77.5
Ca2-VDM	✓	52.1

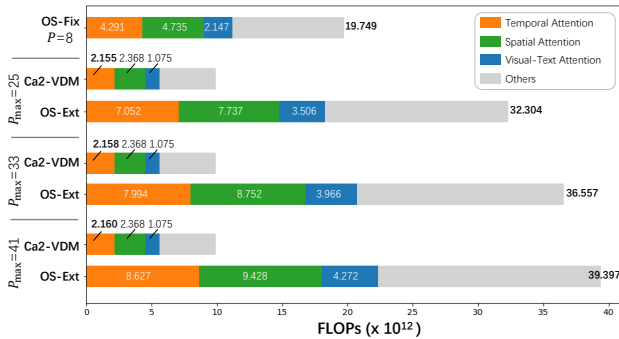


Figure 10. Number of floating-point operations (FLOPs) for generating 56 frames (7 AR steps). All results were computed by conducting only one denoising step for simplicity.

4.3. Evaluation for Autoregression Efficiency

We evaluated the efficiency in two aspects: 1) time cost for autoregressive generation, and 2) detailed computational costs for each component in the Transformer blocks.

Time Cost. We first show the cumulative time cost of autoregressive generation in Table 5. Our models were tested on a single NVIDIA A100 GPU to generate 80 frames at

resolution 256×256 , using improved DDPM [27] with 100 denoising steps. The result of StreamT2V [15] is from its GitHub page, which was tested on the same device and resolution. We can see that Ca2-VDM significantly improved over OS-Fix, OS-Ext, and StreamT2V [15], while being compatible with extendable condition. We further evaluated the accumulated time cost till each AR step, as shown in Figure 8. We can observe that: 1) Compared to OS-Fix, the time cost in Ca2-VDM has a clear reduction since it does not have redundant computations. 2) As the condition extends, the time cost of OS-Ext grows quadratically (before P_{\max} is reached), while the time cost of Ca2-VDM only grows linearly. 3) As the P_{\max} grows to incorporate longer condition, the increase of time cost for OS-Ext is significant, while it is relatively slight for Ca2-VDM.

Computational Cost. We counted the floating-point operations (FLOPs) of temporal, spatial, and visual-text attention layers in the Transformer blocks (*cf.* Figure 10). As the P_{\max} grows, the increased computations are seen in all three types of attention layers for OS-Ext. In contrast, for Ca2-VDM, the number of FLOPs only slightly increases in the temporal attention, while keeping constant in other operations. This is because the extended conditional frames

only participate in the computation as temporal KV-caches.

5. Conclusions

In this paper, we present an efficient autoregressive video diffusion model, *i.e.*, Ca2-VDM. It has two key designs: causal generation and cache sharing. The former eliminates the redundant computations of conditional frames. The latter significantly reduces the storage cost. Our model shows comparable generation quality with existing SOTA VDMs with existing bidirectional attention while achieving notable speedup for the autoregressive generation.

Limitations are left in the Appendix.

References

- [1] Eloi Alonso, Adam Jelley, Vincent Micheli, Anssi Kanervisto, Amos Storkey, Tim Pearce, and François Fleuret. Diffusion for world modeling: Visual details matter in atari. *arXiv preprint arXiv:2405.12399*, 2024. 1
- [2] Andreas Blattmann, Tim Dockhorn, Sumith Kulal, Daniel Mendelevitch, Maciej Kilian, Dominik Lorenz, Yam Levi, Zion English, Vikram Voleti, Adam Letts, et al. Stable video diffusion: Scaling latent video diffusion models to large datasets. *arXiv preprint arXiv:2311.15127*, 2023. 1, 7
- [3] Andreas Blattmann, Robin Rombach, Huan Ling, Tim Dockhorn, Seung Wook Kim, Sanja Fidler, and Karsten Kreis. Align your latents: High-resolution video synthesis with latent diffusion models. In *CVPR*, pages 22563–22575, 2023. 7, 12
- [4] Junsong Chen, YU Jincheng, GE Chongjian, Lewei Yao, Enze Xie, Zhongdao Wang, James Kwok, Ping Luo, Huchuan Lu, and Zhenguo Li. Pixart- α : Fast training of diffusion transformer for photorealistic text-to-image synthesis. In *ICLR*, 2024. 1, 3, 6
- [5] Xinyuan Chen, Yaohui Wang, Lingjun Zhang, Shaobin Zhuang, Xin Ma, Jiashuo Yu, Yali Wang, Dahua Lin, Yu Qiao, and Ziwei Liu. Seine: Short-to-long video diffusion model for generative transition and prediction. In *ICLR*, 2024. 3, 7
- [6] Zuozhuo Dai, Zhenghao Zhang, Yao Yao, Bingxue Qiu, Siyu Zhu, Long Qin, and Weizhi Wang. Animateanything: Fine-grained open domain image animation with motion guidance. *arXiv e-prints*, pages arXiv–2311, 2023. 3, 7
- [7] Alexey Dosovitskiy, Lucas Beyer, Alexander Kolesnikov, Dirk Weissenborn, Xiaohua Zhai, Thomas Unterthiner, Mostafa Dehghani, Matthias Minderer, Georg Heigold, Sylvain Gelly, et al. An image is worth 16x16 words: Transformers for image recognition at scale. In *ICLR*, 2020. 2
- [8] Songwei Ge, Thomas Hayes, Harry Yang, Xi Yin, Guan Pang, David Jacobs, Jia-Bin Huang, and Devi Parikh. Long video generation with time-agnostic vqgan and time-sensitive transformer. In *ECCV*, pages 102–118. Springer, 2022. 7, 12
- [9] Songwei Ge, Seungjun Nah, Guilin Liu, Tyler Poon, Andrew Tao, Bryan Catanzaro, David Jacobs, Jia-Bin Huang, Ming-Yu Liu, and Yogesh Balaji. Preserve your own correlation: A noise prior for video diffusion models. In *ICCV*, pages 22930–22941, 2023. 3, 7, 12
- [10] Rohit Girdhar, Mannat Singh, Andrew Brown, Quentin Duval, Samaneh Azadi, Sai Saketh Rambhatla, Akbar Shah, Xi Yin, Devi Parikh, and Ishan Misra. Emu video: Factorizing text-to-video generation by explicit image conditioning. *arXiv preprint arXiv:2311.10709*, 2023. 3
- [11] Yuwei Guo, Ceyuan Yang, Anyi Rao, Maneesh Agrawala, Dahua Lin, and Bo Dai. Sparsectrl: Adding sparse controls to text-to-video diffusion models. *arXiv preprint arXiv:2311.16933*, 2023. 3
- [12] Yuwei Guo, Ceyuan Yang, Anyi Rao, Zhengyang Liang, Yaohui Wang, Yu Qiao, Maneesh Agrawala, Dahua Lin, and Bo Dai. Animatediff: Animate your personalized text-to-image diffusion models without specific tuning. In *The Twelfth International Conference on Learning Representations*, 2024. 1, 3, 7, 11
- [13] William Harvey, Saeid Naderiparizi, Vaden Masrani, Christian Weilbach, and Frank Wood. Flexible diffusion modeling of long videos. In *NeurIPS*, pages 27953–27965, 2022. 3
- [14] Yingqing He, Tianyu Yang, Yong Zhang, Ying Shan, and Qifeng Chen. Latent video diffusion models for high-fidelity long video generation. *arXiv preprint arXiv:2211.13221*, 2022. 7, 12
- [15] Roberto Henschel, Levon Khachatryan, Daniil Hayrapetyan, Hayk Poghosyan, Vahram Tadevosyan, Zhangyang Wang, Shant Navasardyan, and Humphrey Shi. Streamingt2v: Consistent, dynamic, and extendable long video generation from text. *arXiv preprint arXiv:2403.14773*, 2024. 1, 3, 6, 7, 8, 11
- [16] Jonathan Ho, Ajay Jain, and Pieter Abbeel. Denoising diffusion probabilistic models. In *NeurIPS*, pages 6840–6851, 2020. 1, 3, 11, 12
- [17] Susung Hong, Junyoung Seo, Sunghwan Hong, Heeseong Shin, and Seungryong Kim. Large language models are frame-level directors for zero-shot text-to-video generation. *arXiv e-prints*, pages arXiv–2305, 2023. 3
- [18] Li Hu, Xin Gao, Peng Zhang, Ke Sun, Bang Zhang, and Liefeng Bo. Animate anyone: Consistent and controllable image-to-video synthesis for character animation. *arXiv preprint arXiv:2311.17117*, 2023. 4
- [19] Levon Khachatryan, Andranik Movsisyan, Vahram Tadevosyan, Roberto Henschel, Zhangyang Wang, Shant Navasardyan, and Humphrey Shi. Text2video-zero: Text-to-image diffusion models are zero-shot video generators. In *ICCV*, pages 15954–15964, 2023. 3
- [20] Ilya Loshchilov and Frank Hutter. Decoupled weight decay regularization. In *International Conference on Learning Representations*, 2019. 12
- [21] Haoyu Lu, Guoxing Yang, Nanyi Fei, Yuqi Huo, Zhiwu Lu, Ping Luo, and Mingyu Ding. Vdt: General-purpose video diffusion transformers via mask modeling. In *ICLR*, 2024. 1, 2, 3, 4, 7
- [22] Yu Lu, Linchao Zhu, Hehe Fan, and Yi Yang. Flowzero: Zero-shot text-to-video synthesis with llm-driven dynamic scene syntax. *arXiv preprint arXiv:2311.15813*, 2023. 3

- [23] Zhengxiong Luo, Dayou Chen, Yingya Zhang, Yan Huang, Liang Wang, Yujun Shen, Deli Zhao, Jingren Zhou, and Tieniu Tan. Videofusion: Decomposed diffusion models for high-quality video generation. In *2023 IEEE/CVF Conference on Computer Vision and Pattern Recognition (CVPR)*, pages 10209–10218. IEEE Computer Society, 2023. 7
- [24] Xin Ma, Yaohui Wang, Gengyun Jia, Xinyuan Chen, Ziwei Liu, Yuan-Fang Li, Cunjian Chen, and Yu Qiao. Latte: Latent diffusion transformer for video generation. *arXiv preprint arXiv:2401.03048*, 2024. 1, 3, 4, 6, 7
- [25] Ron Mokady, Amir Hertz, Kfir Aberman, Yael Pritch, and Daniel Cohen-Or. Null-text inversion for editing real images using guided diffusion models. In *CVPR*, pages 6038–6047, 2023. 3
- [26] Chong Mou, Xintao Wang, Liangbin Xie, Yanze Wu, Jian Zhang, Zhongang Qi, and Ying Shan. T2i-adapter: Learning adapters to dig out more controllable ability for text-to-image diffusion models. In *AAAI*, pages 4296–4304, 2024. 3
- [27] Alexander Quinn Nichol and Prafulla Dhariwal. Improved denoising diffusion probabilistic models. In *International conference on machine learning*, pages 8162–8171. PMLR, 2021. 3, 4, 8, 11, 12
- [28] Gyeongrok Oh, Jaehwan Jeong, Sieun Kim, Wonmin Byeon, Jinkyu Kim, Sungwoong Kim, Hyeokmin Kwon, and Sangpil Kim. Mtv: Multi-text video generation with text-to-video models. *arXiv preprint arXiv:2312.04086*, 2023. 3
- [29] William Peebles and Saining Xie. Scalable diffusion models with transformers. In *ICCV*, pages 4195–4205, 2023. 1, 3, 4, 11
- [30] Haonan Qiu, Menghan Xia, Yong Zhang, Yingqing He, Xintao Wang, Ying Shan, and Ziwei Liu. Freenoise: Tuning-free longer video diffusion via noise rescheduling. In *ICLR*, 2024. 1, 3
- [31] Colin Raffel, Noam Shazeer, Adam Roberts, Katherine Lee, Sharan Narang, Michael Matena, Yanqi Zhou, Wei Li, and Peter J Liu. Exploring the limits of transfer learning with a unified text-to-text transformer. *Journal of machine learning research*, 21(140):1–67, 2020. 6
- [32] Weiming Ren, Huan Yang, Ge Zhang, Cong Wei, Xinrun Du, Wenhao Huang, and Wenhui Chen. Consisti2v: Enhancing visual consistency for image-to-video generation. *Transactions on Machine Learning Research*, 2024. 1, 2, 3, 4, 12
- [33] Robin Rombach, Andreas Blattmann, Dominik Lorenz, Patrick Esser, and Björn Ommer. High-resolution image synthesis with latent diffusion models. In *CVPR*, pages 10684–10695, 2022. 1, 3, 6
- [34] Uriel Singer, Adam Polyak, Thomas Hayes, Xi Yin, Jie An, Songyang Zhang, Qiyuan Hu, Harry Yang, Oron Ashual, Oran Gafni, et al. Make-a-video: Text-to-video generation without text-video data. In *ICLR*, 2023. 7
- [35] Ivan Skorokhodov, S Tulyakov, and Mohamed Elhoseiny. Stylegan-v: A continuous video generator with the price, image quality and perks of stylegan2. 2022 ieee. In *CVPR*, pages 3616–3626, 2021. 12
- [36] Jascha Sohl-Dickstein, Eric Weiss, Niru Maheswaranathan, and Surya Ganguli. Deep unsupervised learning using nonequilibrium thermodynamics. In *International conference on machine learning*, pages 2256–2265. PMLR, 2015. 3
- [37] Jiaming Song, Chenlin Meng, and Stefano Ermon. Denoising diffusion implicit models. In *ICLR*, 2021. 1, 3
- [38] Yang Song, Jascha Sohl-Dickstein, Diederik P Kingma, Abhishek Kumar, Stefano Ermon, and Ben Poole. Score-based generative modeling through stochastic differential equations. In *ICLR*, 2021. 1
- [39] Khurram Soomro, Amir Roshan Zamir, and Mubarak Shah. Ucf101: A dataset of 101 human actions classes from videos in the wild. *arXiv preprint arXiv:1212.0402*, 2012. 2, 7, 12
- [40] Thomas Unterthiner, Sjoerd van Steenkiste, Karol Kurach, Raphaël Marinier, Marcin Michalski, and Sylvain Gelly. Fvd: A new metric for video generation. In *ICLR 2019 Workshop DeepGenStruct*, 2019. 7, 12
- [41] Vikram Voleti, Alexia Jolicoeur-Martineau, and Chris Pal. Mcvd - masked conditional video diffusion for prediction, generation, and interpolation. In *NeurIPS*, pages 23371–23385. Curran Associates, Inc., 2022. 3, 7
- [42] Fu-Yun Wang, Wenshuo Chen, Guanglu Song, Han-Jia Ye, Yu Liu, and Hongsheng Li. Gen-l-video: Multi-text to long video generation via temporal co-denoising. *arXiv preprint arXiv:2305.18264*, 2023. 3, 6, 7, 8
- [43] Jiuniu Wang, Hangjie Yuan, Dayou Chen, Yingya Zhang, Xiang Wang, and Shiwei Zhang. Modelscope text-to-video technical report. *arXiv preprint arXiv:2308.06571*, 2023. 1, 3, 7, 11
- [44] Xiang Wang, Hangjie Yuan, Shiwei Zhang, Dayou Chen, Jiuniu Wang, Yingya Zhang, Yujun Shen, Deli Zhao, and Jingren Zhou. Videocomposer: Compositional video synthesis with motion controllability. *NeurIPS*, 36, 2023. 7
- [45] Yi Wang, Yanan He, Yizhuo Li, Kunchang Li, Jiashuo Yu, Xin Ma, Xinhao Li, Guo Chen, Xinyuan Chen, Yaohui Wang, et al. Internvid: A large-scale video-text dataset for multimodal understanding and generation. In *ICLR*, 2024. 6, 11
- [46] Wenming Weng, Ruoyu Feng, Yanhui Wang, Qi Dai, Chunyu Wang, Dacheng Yin, Zhiyuan Zhao, Kai Qiu, Jianmin Bao, Yuhui Yuan, et al. Art-v: Auto-regressive text-to-video generation with diffusion models. *arXiv preprint arXiv:2311.18834*, 2023. 3
- [47] Jun Xu, Tao Mei, Ting Yao, and Yong Rui. Msr-vtt: A large video description dataset for bridging video and language. In *CVPR*, pages 5288–5296, 2016. 2, 7, 12
- [48] Sihyun Yu, Jihoon Tack, Sangwoo Mo, Hyunsu Kim, Junho Kim, Jung-Woo Ha, and Jinwoo Shin. Generating videos with dynamics-aware implicit generative adversarial networks. In *International Conference on Learning Representations*, 2022. 7
- [49] Sihyun Yu, Kihyuk Sohn, Subin Kim, and Jinwoo Shin. Video probabilistic diffusion models in projected latent space. In *CVPR*, pages 18456–18466, 2023. 7
- [50] Yan Zeng, Guoqiang Wei, Jiani Zheng, Jiabin Zou, Yang Wei, Yuchen Zhang, and Hang Li. Make pixels dance: High-dynamic video generation. *arXiv preprint arXiv:2311.10982*, 2023. 3, 7, 12

- [51] Jiangning Zhang, Chao Xu, Liang Liu, Mengmeng Wang, Xia Wu, Yong Liu, and Yunliang Jiang. Dtvnet: Dynamic time-lapse video generation via single still image. In *European Conference on Computer Vision*, pages 300–315. Springer, 2020. 2, 6, 7, 12
- [52] Lvmin Zhang, Anyi Rao, and Maneesh Agrawala. Adding conditional control to text-to-image diffusion models. In *CVPR*, pages 3836–3847, 2023. 3
- [53] Shiwei Zhang, Jiayu Wang, Yingya Zhang, Kang Zhao, Hangjie Yuan, Zhiwu Qin, Xiang Wang, Deli Zhao, and Jingren Zhou. I2vgen-xl: High-quality image-to-video synthesis via cascaded diffusion models. *arXiv preprint arXiv:2311.04145*, 2023. 3, 11
- [54] Yabo Zhang, Yuxiang Wei, Dongsheng Jiang, XIAOPENG ZHANG, Wangmeng Zuo, and Qi Tian. Controlvideo: Training-free controllable text-to-video generation. In *ICLR*, 2024. 3
- [55] Zangwei Zheng, Xiangyu Peng, Tianji Yang, Chenhui Shen, Shenggui Li, Hongxin Liu, Yukun Zhou, Tianyi Li, and Yang You. Open-sora: Democratizing efficient video production for all, 2024. 1, 6, 11

Appendix

Table of Content

- Sec. A: Limitations and Possible Future Directions
- Sec. B: Training Objectives
- Sec. C: Training Details and Hyperparameters
- Sec. D: Evaluation Details

A. Limitations and Possible Future Directions

We analyze the limitations of the current work and propose some possible directions for future work.

Causal Modeling in Pretraining. Currently, all the pre-trained weights for video diffusion models (either UNet-based, *e.g.*, ModelScore-T2V [43], AnimateDiff [12], or Transformer-based, *e.g.*, Open-Sora [55]) use bidirectional attention in their temporal modules. Our Ca2-VDM is built upon Open-Sora which was also pretrained using bidirectional attention. However, finetuning these bidirectionally pre-trained temporal modules using causal attention might be sub-optimal. The weights between bidirectional and causal temporal attention layers might have inherent gaps. Due to the limited computational resources, we did not conduct causal pretraining. Pretraining the VDM’s temporal modules from scratch (using causal attention) might have potential improvements.

Training Efficiency Trade-off. Ca2-VDM uses extendable conditional frames and cyclic TPEs. These designs require the model to learn all the possible situations during training. Compared to fixed-length conditional frames and conventional TPEs, the model needs more time to achieve training convergence. Meanwhile, the longer maximum condition length (*i.e.*, P_{\max}) we use, the more training is

required. On the other hand, once the model is trained, it is more powerful for integrating long-term context. Consequently, it’s also potentially beneficial for long-term autoregressive video generation.

Quality Degradation in Long-term Generation. As a common challenge, VDMs in long-term autoregressive generation suffer from frame appearance changes and quality degradation. Some works [15, 53] mitigate this issue by providing the VDM with the global appearance information extracted from the initial frame. However, during the long-term generation, video content may change and not all frames commit the same global appearance. In our setting, the long-term extendable context (*i.e.*, early context from the KV-cache queue) helps mitigate the quality degradation, demonstrated by the results in Table 3 and Table 4. Further research on approaches addressing quality degradation is warranted and may hold potential significance for long-term video generation.

B. Training Objectives

Recall that (*cf.* Sec. 3.2 in the main text) existing diffusion models [16, 27, 29] are trained with the variational lower bound of z_0 ’s log-likelihood, formulated as

$$\mathcal{L}_{\text{vib}}(\theta) = -\log p_{\theta}(z_0|z_1) + \sum_t D_{KL}(q(z_{t-1}|z_t, z_0)||p_{\theta}(z_{t-1}|z_t)). \quad (6)$$

Since q and p_{θ} are both Gaussian, D_{KL} is determined by the mean μ_{θ} and covariance Σ_{θ} . By re-parameterizing μ_{θ} as a noise prediction network ϵ_{θ} and fixing Σ_{θ} as a constant variance schedule [16], the model can be trained using a simplified objective function:

$$\mathcal{L}_{\text{simple}}(\theta) = \mathbb{E}_{z, \epsilon, t} [\|\epsilon_{\theta}(z_t, t) - \epsilon\|_2^2], \quad \epsilon \sim \mathcal{N}(0, 1). \quad (7)$$

In our setting, the simplified objective function is

$$\tilde{\mathcal{L}}_{\text{simple}}(\theta) = \mathbb{E}_{z, \epsilon, t} [\|(\epsilon_{\theta}([z_0^{0:P}, z_t^{P:L}], t) - \epsilon) \odot m\|_2^2]. \quad (8)$$

Following prior works [27, 29], we train the model with learnable covariance Σ_{θ} to improve the sampling quality. This is achieved by optimizing the full D_{KL} term in \mathcal{L}_{vib} , resulting in an $\tilde{\mathcal{L}}_{\text{vib}}$ in our setting, *i.e.*, applied with the same timestep vector t and loss mask m . Then, the model is optimized by a combined loss function $\tilde{\mathcal{L}}_{\text{simple}} + \tilde{\mathcal{L}}_{\text{vib}}$.

C. Training Details and Hyperparameters

Text-to-Video (T2V) Training. We trained Ca2-VDM and the OS-Fix baseline on a large-scale video-text dataset InternVid [45], by filtering it to a sub-set of 4.9M high-quality video-text pairs with resolution 256×256. For Ca2-VDM, the training consists of two stages. We first train

the causal modeling ability without the clean prefix (*i.e.*, without conditional frames) on 32-frame videos. Then we use longer videos of 65 frames to train the model with the clean prefix, *i.e.*, with $l = 16$, $P_{\max} = 1 + 3l = 49$ and $\max(L_{\text{train}}) = P_{\max} + l = 65$. In the first stage, the model was trained with a batch size of 288 for 32k steps. In the second stage, it was trained with a batch size of 144 for 21k steps. For OS-Fix, it was trained with $L_{\text{train}} = 32$ frames and $P = l = L_{\text{train}}/2 = 16$ frames, *i.e.*, the prefix length is fixed. It was trained with a batch size of 288 for 20k steps ⁴.

Video Prediction Training. We trained OS-Fix, OS-Ext, and Ca2-VDM on the SkyTimelapse [51] dataset at resolution 256×256 with $l = 8$. OS-Ext and Ca2-VDM both used $P_{\max} = 1 + 3l = 25$ (*i.e.*, $L_{\text{train}} = 33$). OS-Fix used a fixed $P = 8$ and $L_{\text{train}} = 16$. All three models were trained with a batch size of 8 for 11k steps ⁵.

Hyperparameters. For all the training, we used the DDPM [16] schedule with $T = 1000$, $\beta_1 = 10^{-4}$, and $\beta_T = 0.02$. The models were trained using AdamW [20] optimizer with a learning rate of $2e-5$. At the inference stage, we used the improved DDPM schedule [27] with 100 steps. For text-to-video, we set the classifier-free guidance scale as 7.5.

D. Evaluation Details

D.1. Datasets

MSR-VTT [47]. we used its official test split which contains 2990 videos, with 20 manually annotated captions for each video. Following prior works [32, 50] and for fair comparisons, we randomly selected a caption for each video and generated 2990 videos for evaluation.

UCF101 [39]. As it only contains label names, we employed the descriptive text prompts from PYoCo [9], and generated 2048 samples with uniform distribution for each category following [9, 14, 32].

SkyTimelapse [51]. It is a time-lapse dataset showing dynamic sky scenes (*e.g.*, cloudy sky with moving clouds). We used it for video prediction (*i.e.*, without text input). Its training set contains 997 long timelapse videos, which are cut into 2392 short videos. Its test set contains 111 long timelapse videos, which are cut into 225 short videos. We trained the models on its training set and evaluated them on its test set.

D.2. Quantitative Evaluation

Fréchet Video Distance (FVD) [40] measures the similarity between generated and real videos based on the distributions on the feature space. We followed prior works [3, 8,

32] to use a pretrained I3D model⁶ to extract the features. We used the codebase⁷ from StyleGAN-V [35] to compute FVD statistics.

For the autoregressive generation results (*e.g.*, the results in Table 3 and Table 4), we calculated the chunk-wise FVD. Specifically, for Table 3, each model generated 48 frames with 6 AR steps and $l = 8$. Since the I3D model accepts at least 16 frames, we evaluated the FVD scores of three 16-frame chunks (*i.e.*, 2 AR steps in each) w.r.t. the 16-frame ground-truth videos. For Table 4, each model generated 96 frames with 6 AR steps and $l = 16$. We evaluated the FVD scores of the generated 16-frame chunk from each AR step w.r.t. the first AR step. Each model generated 512 videos for FVD calculation.

⁴OS-Fix converges faster than Ca2-VDM since it only needs to learn fixed-length conditional frames.

⁵In contrast to text-to-video, the video prediction task on the SkyTime-lapse dataset has less diversity and converges faster. So we used smaller batch size and training steps.

⁶https://github.com/songweige/TATS/blob/main/tats/fvd/i3d_pretrained_400.pt

⁷<https://github.com/universome/stylegan-v>